G protein-coupled odorant receptors underlie mechanosensitivity in mammalian olfactory sensory neurons

Timothy Connelly[a,1], Yiqun Yu[a,1], Xavier Grosmaitre[a,b], Jue Wang[a], Lindsey C. Santarelli[a], Agnes Savigner[a], Xin Qiao[a], Zhenshan Wang[c,d], Daniel R. Storm[d], and Minghong Ma[a,2]

[a]Department of Neuroscience, University of Pennsylvania Perelman School of Medicine, Philadelphia, PA 19104; [b]CNRS, Université de Bourgogne, 21000 Dijon, France; [c]College of Life Science, Hebei University, Baoding 071002, China; and [d]Department of Pharmacology, University of Washington School of Medicine, Seattle, WA 98195

Edited* by John R. Carlson, Yale University, New Haven, CT, and approved December 8, 2014 (received for review September 25, 2014)

Mechanosensitive cells are essential for organisms to sense the external and internal environments, and a variety of molecules have been implicated as mechanical sensors. Here we report that odorant receptors (ORs), a large family of G protein-coupled receptors, underlie the responses to both chemical and mechanical stimuli in mouse olfactory sensory neurons (OSNs). Genetic ablation of key signaling proteins in odor transduction or disruption of OR–G protein coupling eliminates mechanical responses. Curiously, OSNs expressing different OR types display significantly different responses to mechanical stimuli. Genetic swap of putatively mechanosensitive ORs abolishes or reduces mechanical responses of OSNs. Furthermore, ectopic expression of an OR restores mechanosensitivity in loss-of-function OSNs. Lastly, heterologous expression of an OR confers mechanosensitivity to its host cells. These results indicate that certain ORs are both necessary and sufficient to cause mechanical responses, revealing a previously unidentified mechanism for mechanotransduction.

odorant receptors | mechanical sensors | G protein-coupled receptors | mechanotransduction | heterologous expression

Mechanosensitive cells that convert physical force into biochemical or electrical signals play critical roles in sensing the external and internal environments. A variety of molecules have been implicated as mechanical sensors in different cell types (1–3), but our understanding of the mechanical sensors is still limited. We previously discovered that some OSNs in the mammalian nose responded to mechanical stimulation (4), a feature that may allow the nose to carry an afferent signal of breathing to the brain and facilitate binding of orofacial sensation (5). In the current study, we aim to identify the mechanical sensor(s) and mechanotransduction pathway in OSNs.

In mammals, smell perception depends on a large family of ORs expressed in OSNs. Out of a repertoire of >1,000 ORs (6, 7), each OSN expresses a single type, which determines its response profile and central target in the brain. Binding of odorant molecules with specific ORs activates the olfactory G protein G_{olf}, which in turn activates type III adenylyl cyclase (ACIII). ACIII activation causes increased production of cAMP, which opens a cyclic nucleotide-gated cation (CNG) channel. The inward current via the CNG channel is further amplified by Cl^- outflow through a calcium-activated Cl^- channel. This transduction cascade leads to depolarization of OSNs, which fire action potentials carrying the odor information to the brain (8). OSNs expressing the same OR are scattered in one of the few broadly defined zones in the olfactory epithelium, but their axons typically converge onto a pair of glomeruli in the olfactory bulb (9).

Here we report that disruption of the olfactory signal transduction cascade completely eliminates mechanical responses in OSNs. OSNs expressing different receptor types display differential responses to mechanical stimuli. For instance, I7, M71, and SR1 neurons have much stronger mechanical responses than MOR23 and mOR-EG neurons. Loss-of-function mutation of the I7 receptor, genetic switch of the M71 receptor, or ablation of the SR1 receptor, abolishes or dramatically reduces mechanical responses in the host OSNs. Furthermore, ectopic expression of the I7 receptor restores mechanosensitivity in loss-of-function mutant I7 cells. Finally, heterologous expression of SR1 confers mechanosensitivity to its host cells. Our findings suggest that G protein-coupled receptors (GPCRs) may have an overlooked function as mechanosensors in neurons and add to the growing list of polymodal transmembrane receptors in sensory organs.

Results

The Olfactory Signal Transduction Cascade Underlies Mechanical Responses in OSNs. We recently discovered that a subset of mouse OSNs exhibited responses to both odor and mechanical force, but these responses were absent in OSNs from CNG channel knockout mice (4). To determine whether the odor transduction cascade underlies both chemical and mechanical sensitivity in OSNs, we tested whether ablating targets upstream of the CNG channel would also eliminate mechanical responses.

We first examined mechanical responses of mouse OSNs from ACIII knockout mice (10) to determine whether ACIII is required for mechanotransduction. Our previous study revealed that ~70% (184 of 258) of wild-type cells in the septal organ, an isolated patch of olfactory epithelium at the base of the nasal septum, exhibited mechanosensory responses to puffs of Ringer's solution. Here we recorded odorant and mechanical responses

Significance

Mechanical stimuli (pressure, shear stress, membrane stretch, etc.) are a basic form of stimulation that can induce physiological responses in many body organs (skin, muscle, ear, lung, airway, kidney, blood vessels, etc.). The current dogma in sensory systems is that mechanical stimuli are mainly transduced by force-gated ion channels. Our study reveals a previously unidentified cascade for mechanotransduction in neurons and suggests that G protein-coupled receptors may have an overlooked function as mechanical sensors. This finding establishes a molecular mechanism through which the nose sends an afferent signal of breathing to the brain to facilitate integration of orofacial sensation and synchronize delta/theta-band activity in certain brain regions with respiration.

Author contributions: T.C., Y.Y., X.G., and M.M. designed research; T.C., Y.Y., X.G., J.W., L.C.S., A.S., and X.Q. performed research; Z.W. and D.R.S. contributed new reagents/analytic tools; T.C., Y.Y., X.G., J.W., L.C.S., and M.M. analyzed data; and T.C., Y.Y., X.G., and M.M. wrote the paper.

The authors declare no conflict of interest.

*This Direct Submission article had a prearranged editor.

[1]T.C. and Y.Y. contributed equally to this work.

[2]To whom correspondence should be addressed. Email: minghong@mail.med.upenn.edu.

This article contains supporting information online at www.pnas.org/lookup/suppl/doi:10.1073/pnas.1418515112/-/DCSupplemental.

from the dendritic knobs of individual OSNs in the septal organ using perforated patch clamp recordings. In all, 58% (11 of 19) of ACIII$^{+/+}$ and ACIII$^{+/-}$ neurons exhibited robust inward transduction currents in response to mechanical stimulation ($P = 0.30$ in Fisher's exact test compared with our previous data on wild-type cells). As expected, these neurons also showed robust responses to IBMX (3-isobutyl-1-methyl-xanthine), a potent phosphodiesterase inhibitor that elevates the intracellular cAMP level, as well as to odors (Fig. 1*A*). When we applied the mechanical stimulation to septal organ neurons ($n = 21$) from ACIII$^{-/-}$ mice, however, we did not observe a single response (c.f. Fig. 1 *A* and *D*; $P < 0.0001$, Fisher's exact test). Nor did these neurons respond to odors or IBMX (Fig. 1*D*). The lack of IBMX responses suggests that the basal cAMP level in ACIII$^{-/-}$ neurons was negligible due to the loss of ACIII activity, and therefore blocking phosphodiesterase activity had little effect. ACIII$^{-/-}$ neurons exhibited larger voltage-gated ionic currents elicited by the same voltage steps (Fig. 1 *B* and *E*) and fired at higher frequency in response to the same current injection (Fig. 1 *C* and *F*). The higher excitability is presumably attributed to functional compensation for the loss of ACIII mediated activity in these cells. These results indicate that ACIII is required for mechanosensitivity in OSNs (11), consistent with the pharmacological evidence obtained by an adenylyl cyclase blocker (4).

We next examined whether OR activation of G protein itself was required for mechanosensitivity in OSNs. ORs are rhodopsin-like type A GPCRs, which contain a tripeptide motif, Asp-Arg-Tyr (DRY), near the cytoplasmic end of transmembrane domain III that is required for coupling of the receptors to G proteins (12–14). Expression of a mutant I7 receptor in which the DRY sequence was changed to RDY eliminates odor responses in these I7-RDY neurons (15), suggesting this is an effective method of blocking receptor-G protein activation.

We recorded from neurons expressing either wild-type I7 or mutant I7-RDY along with a fluorescent marker (see *Materials and Methods* for details). Wild-type I7 neurons ($n = 12$ under cell-attached configuration and $n = 4$ under perforated patch clamp) displayed spontaneous firing and robust mechanical responses elicited by puffs of Ringer's solution (Fig. 2 *A* and *B*). Because these cells fired irregularly, delivery of puff stimulation was mostly in a stochastic manner, even though we attempted to apply stimulation after a spontaneous burst (if there was an obvious one). A puff typically elicited a response after a latency of 100–200 ms, which is characterized by an initial burst (*b*) of

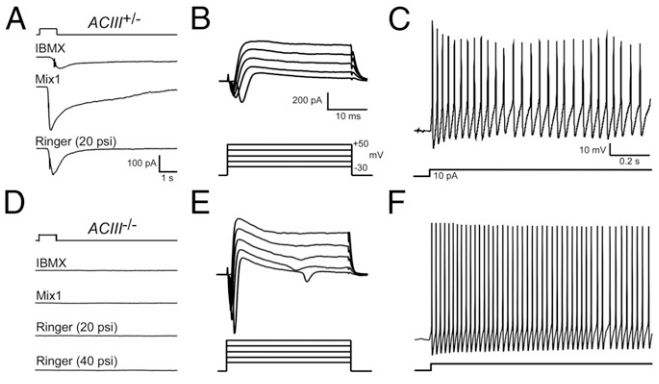

Fig. 1. ACIII is required for mechanical responses of OSNs. (*A*–*C*) A septal organ OSN from a heterozygous ACIII$^{+/-}$ mouse responded to puffs of IBMX (100 μM), Mix 1 (10 μM), or Ringer's solution (all at 20 psi) under voltage-clamp mode (*A*). The same cell exhibited voltage-gated ionic currents (*B*) and action potentials elicited by a depolarizing current (*C*). (*D*–*F*) A septal organ OSN from a homozygous ACIII$^{-/-}$ mouse failed to respond to puffs of IBMX, Mix 1 or Ringer's solution (20 psi if not stated otherwise). The same cell exhibited voltage-gated ionic currents (*E*) and action potentials elicited by a depolarizing current (*F*). The holding potential was −60 mV for all cells. The scale bars in *A*–*C* apply to the same column in *D*–*F*.

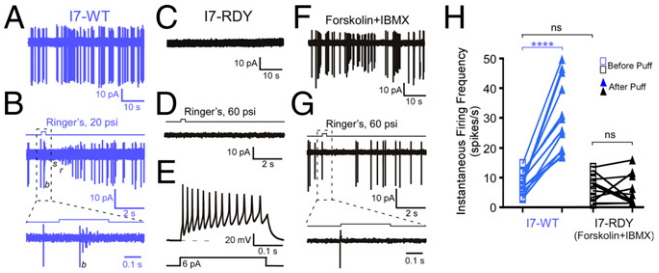

Fig. 2. OR–G protein coupling is required for mechanical responses of OSNs. (*A* and *B*) Wild-type I7 neurons (I7-WT) exhibited spontaneous action potentials (*A*) and responses to puffs of Ringer's solution (*B*). Note different time scales in *A* and *B*. (*C*–*E*) I7-RDY neurons failed to show spontaneous action potentials (*C*) and responses to puffs of Ringer's solution (*D*), but fired action potentials in response to a depolarizing current of −6 pA (*E*). In E, the cell was held at −60 mV before the current injection. (*F* and *G*) Brief application of forskolin (10 μM) and IBMX (100 μM) caused I7-RDY neurons to fire action potentials for minutes (*F*). Under such condition, I7-RDY neurons did not respond to puffs of Ringer's solution (*G*). Note different time scales in *F* and *G*. Cell-attached patch recordings were performed in all panels except for *E*, where perforated patch clamp was used. (*H*) Summary of the instantaneous firing frequency before and after onset of the puff in I7-WT and I7-RDY neurons with elevated "basal" activity. Puffs were delivered at 20 psi for I7-WT cells and 20–60 psi for I7-RDY cells. When multiple trials were tested in a single cell, the firing frequency was averaged from these trials. Paired *t* test was used for the two conditions within each cell type and unpaired *t* test was used for the basal activity between the two cell types. ****$P < 0.0001$ and ns = not significant.

four to six spikes with decreasing amplitude, followed by a silent (*s*) period and then a rebound (*r*) phase containing spikes with increasing amplitude (Fig. 2*B*), similar to odor induced responses in OSNs (16, 17). Such a firing pattern was never observed in spontaneous bursts of I7 neurons. The instantaneous firing frequency increased from the basal level of 8.2 ± 1.0 Hz to 30.3 ± 3.5 Hz ($n = 12$) during puff-induced bursts (Fig. 2*H*; see *Materials and Methods* for details). Note that the basal firing rates of I7 neurons measured this way was very similar to the overall spontaneous firing rates analyzed for much longer periods of time from our previous study (8.9 ± 0.9 Hz, $n = 21$) (16). In sharp contrast, I7-RDY neurons ($n = 10$ under cell-attached configuration and $n = 7$ under perforated patch clamp) showed neither spontaneous firing nor puff-induced responses (Fig. 2 *C* and *D*; $P < 0.0001$, Fisher's exact test). Typical voltage-gated ionic currents as well as action potentials in response to depolarizing current in I7-RDY neurons indicate they are healthy and capable of firing (Fig. 2*E* and Fig. S1). These results suggest that OR–G protein coupling either underlies the mechanical responses or plays a permissive role in this process. To differentiate these two possibilities, we applied brief puffs of forskolin (an activator of adenylyl cyclase at 10 μM) and IBMX (100 μM) to elevate the cAMP level in I7-RDY neurons and titrate the "basal" activity to a level comparable to that in wild-type I7 neurons (Fig. 2 *F* and *H*). Puffs of Ringer's solution never elicited a characteristic response as seen in wild-type I7 neurons. In the example shown in Fig. 2*G*, a puff did not elicit any action potentials within 200 ms in an I7-RDY neuron. These cells showed similar instantaneous firing frequencies before or after onset of the puffs (before: 6.4 ± 1.4 Hz vs. after: 5.7 ± 1.7 Hz, $n = 10$) (Fig. 2*H*). These results indicate that I7-RDY neurons, even with elevated "basal" firing frequencies, did not display puff-induced responses, suggesting that OR–G protein coupling plays a direct role in mediating mechanosensitivity of OSNs.

G Protein-Coupled ORs Are Necessary and Sufficient for Mechanical Responses of OSNs. Because only a subset of OSNs in the olfactory epithelium displays mechanosensitivity, whereas all I7 neurons do, we suspect that ORs could be classified based on sensitivity to mechanical stimulation. We therefore examined mechanical responses in genetically labeled OSNs expressing each of these

NEUROSCIENCE

five receptors: SR1, I7, M71, MOR23, or mOR-EG, which have been extensively studied in gene-targeted or transgenic mice (18–21).

We applied puffs of Ringer's solution at different pressures to generate stimulus-response relationships for neurons expressing each receptor type. OSNs expressing SR1 (n = 11 under perforated patch clamp), I7 (n = 12 under cell-attached configuration and 4 under perforated patch clamp), and M71 (11 under cell-attached configuration and 9 under perforated patch clamp) exhibited increasing responses to increasing pressure stimuli (Fig. 3 *A*–*C*). Indeed, these OSNs showed similar stimulus-response relationship (Fig. 3*F*). Conversely, neurons that expressed either MOR23 (n = 9) or mOR-EG (n = 9) were mostly insensitive to puffs of Ringer's solution (Fig. 3 *D*–*F*). However, all MOR23 and mOR-EG neurons responded to their cognate ligands (Fig. 3 *D* and *E*). These results further support the notion that receptor type determines mechanosensitivity of OSNs.

We then examined whether genetic ablation or switch of a putatively mechanosensitive OR eliminates mechanical responses. First, we used a mouse line in which the coding sequence of SR1 is replaced with that of monomeric red fluorescent protein (RFP) (20). SR1 neurons are mechanosensitive (Fig. 3 *A* and *F*) and make up 50% of all cells in the septal organ (22). Because ΔSR1-RFP neurons cannot express SR1, they must "choose" another functional OR to express (23). We expect that only a subset of ΔSR1-RFP neurons will respond to mechanical stimuli, because only those neurons that "choose" another mechanosensitive receptor would do so. To facilitate a direct comparison between the two cell groups, we kept the ejection pressure at 20 psi to reduce variations in stimulation. We found that the percentage of cells responding to puffs of Ringer's solution was sharply reduced in ΔSR1-RFP cells (2 of 12 = 17%), in contrast to SR1 cells (10 of 11 = 91%; $P < 0.001$, Fisher's exact test) (Fig. 4*A*). Second, we used another mouse line in which the coding sequence of M71 is replaced with that of β2 adrenergic receptor (β2AR) (24, 25), a nonmechanosensitive GPCR (26, 27). In contrast to M71 neurons (n = 7 tested at 20 psi), β2AR→M71 neurons (n = 7; $P < 0.001$, Fisher's exact test) failed to respond to puffs of Ringer's solution or acetophenone (a ligand for M71), but did respond to the β2AR agonist isoproterenol (Fig. 4*B*). These findings indicate that SR1 and M71 are required for mechanosensitivity of their host OSNs.

To determine whether ORs are sufficient to confer mechanosensitivity to OSNs, we used a genetic approach to rescue the function of I7-RDY cells. By breeding I7-RDY-IRES-YFP mice onto the homozygous ubiquitous I7 (Ub-I7) background, we obtained neurons that expressed the inactive I7-RDY receptor

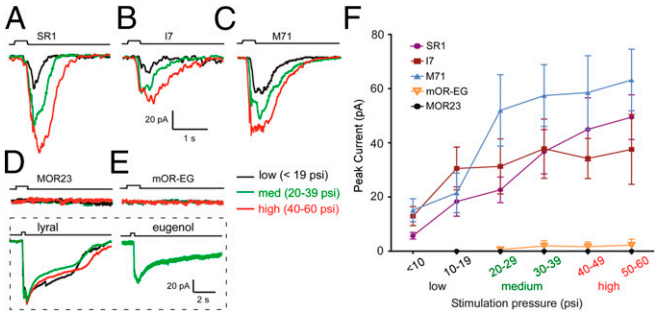

Fig. 3. OR type determines mechanosensitivity of OSNs. (*A*–*C*) An SR1 (*A*), I7 (*B*), or M71 (*C*) neuron showed increasing transduction currents to increasing pressure stimuli. (*D* and *E*) An MOR23 (*D*) or mOR-EG (*E*) neuron did not respond to puffs of Ringer's solution at any pressure, but responded consistently to the cognate ligand lyral (independent of delivery pressure) or eugenol, respectively. (*F*) Summary of the mechanical responses for each receptor type. Only recordings from perforated patch clamp configuration were included here and all recordings were under voltage-clamp mode with a holding potential of −60 mV. Error bars = SEM. Scale bars in *B* apply to all traces except those within the dotted rectangle.

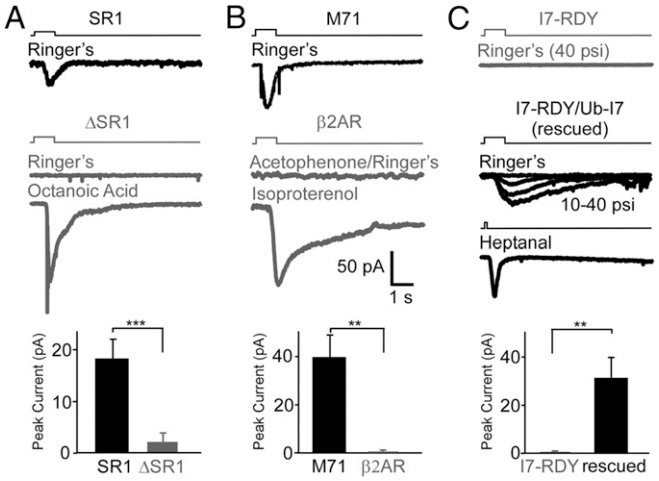

Fig. 4. ORs are necessary and sufficient for mechanosensitivity of OSNs. (*A*) Genetic ablation of SR1 drastically reduced the mechanical responses to puffs of Ringer's solution in the host OSNs. The puff-induced responses in ΔSR1-RFP cells (2.08 ± 1.75 pA) were significantly smaller than those in SR1 cells (18.12 ± 3.86 pA; $P < 0.001$ in nonparametric, unpaired Mann–Whitney test). (*B*) Genetic replacement of the M71 receptor by β2AR enabled the host OSNs to respond to isoproterenol, but abolished responses to puffs of acetophenone or Ringer's solution. The puff-induced responses in β2AR cells (0.76 ± 0.68 pA) were significantly smaller than those in M71 cells (39.49 ± 8.87 pA; $P < 0.01$ in nonparametric, unpaired Mann–Whitney test). All puffs in *A* and *B* were at 20 psi. (*C*) Ectopic expression of the I7 receptor restores the mechanical and odorant responses in I7-RDY cells. The puff-induced responses in I7-RDY cells (0.57 ± 0.29 pA; n = 7 under perforated patch clamp) were significantly smaller than those in I7-RDY/Ub-I7 cells (31.08 ± 8.00 pA; $P < 0.01$ in nonparametric, unpaired Mann–Whitney test). The graph summarizes data obtained at 40 psi because of the relatively small size at 20 psi. Heptanal was delivered at 20 psi for 100 ms, a brief puff that did not elicit mechanical responses. All compounds were at 100 μM. Error bars = SEM.

as well as wild-type I7 driven by the OMP gene (see *Materials and Methods* for details). In sharp contrast to I7-RDY neurons (n = 17, see above), I7-RDY/Ub-I7 neurons responded to puffs of Ringer's solution (n = 8; $P < 0.0001$, Fisher's exact test) as well as to heptanal (n = 9), an I7 ligand (Fig. 4*C*). Therefore, ectopic expression of the I7 receptor rescues both odorant and mechanical responses in loss-of-function I7-RDY neurons.

Although the above findings are consistent with the notion that some ORs including I7 serve as mechanosensors, they do not completely rule out the possibility that these ORs merely transduce signals from an unidentified mechanosensor and the heterogeneity of OSN mechanosensitivity arises from the differential expression of the bona fide mechanosensor. If this were true, one may expect that the percentage of mechanosensitive OSNs in Ub-I7 mice would be similar to that from wild-type animals. We performed patch clamp recordings from randomly selected OSNs in Ub-I7 mice and found that 92.0% (23 out of 25) responded to puffs of Ringer's solution. This percentage is significantly higher than that obtained from wild-type mice (49% or 18 out of 37 neurons; $P < 0.001$ in Fisher's exact test) (Fig. S2). The two nonresponsive cells could be due to low or no expression of OMP (and thus I7) and/or other undefined reasons. These results support that the I7 receptor serves as a mechanosensor per se, rather than a transducer for another mechanosensor.

We suspect that puffs of Ringer's solution can potentially disturb the chemical environment surrounding OSNs in the intact epithelium, so that the observed responses might be due to OR activation by chemical rather than mechanical stimuli. To rule out this possibility, we repeated the same puffing test on dissociated OSNs (Fig. S3). Out of 53 randomly chosen mature OSNs from heterozygous OMP-GFP mice (28), 21 (or 40%) showed responses (>5 pA) to puffs of Ringer's solution. The

response properties (including latency, kinetics, and adaptation) and the fraction of responsive cells are similar to those observed from OSNs situated in the intact epithelium (49%, 18 out of 37 neurons; $P = 0.51$, Fisher's exact test). This finding supports that puff-induced responses from in situ OSNs most likely result from mechanical stimulation.

Heterologous Expression of SR1 Is Sufficient to Cause Mechanosensitivity. To provide direct evidence that ORs are mechanosensitive, we used a heterologous gene transfer approach in Hana3A cells, a modified HEK293 cell line optimized for OR surface expression (29–31). Using a Ca^{2+} sensitive indicator fluo-4, we monitored intracellular Ca^{2+} levels of Hana3A cells transfected by Rho-tagged *SR1* or *mOR-EG* receptor gene upon mechanical stimulation. Rho-tag facilitates OR surface expression and allows assessment of the transfection efficiency (~80%) via a Rho antibody in live-cell immunocytochemistry (Fig. 5*A*). Puffs of Ringer's solution elevated the Ca^{2+} levels in Hana3A cells transfected with *Rho-SR1* ($\Delta F/F = 0.46 \pm 0.09$, mean ± SEM, $n = 16$ cells from four plates), but not in those transfected with *Rho-mOR-EG* ($\Delta F/F = 0.04 \pm 0.01$, $n = 11$ cells from three plates) (Fig. 5 *B* and *D*), consistent with the patch clamp recordings in native OSNs (Fig. 3). To directly visualize $SR1^+$ cells and to rule out a potential role of Rho-tag in the observed mechanosensitivity, we next made an adenovirus carrying untagged SR1, which drives coexpression of a red fluorescent marker mCherry under the bicistronic control of internal ribosome entry site (IRES). Viral delivery of SR1 produced similar results: Increased Ca^{2+} levels were only observed in Hana3A cells infected by adenovirus carrying SR1-IRES-mCherry (Ad-SR1-mCherry: $\Delta F/F = 0.61 \pm 0.06$, $n = 13$ from four plates) but not mCherry alone (Ad-mCherry: $\Delta F/F = 0.03 \pm 0.02$, $n = 10$ from three plates) (Fig. 5 *C* and *D*). Occasionally in a single plate infected by SR1-IRES-mCherry virus, we found both $SR1^+$ (red) and $SR1^-$ (nonred) cells within a single imaging field and only $SR1^+$ cells showed responses to puffs of Ringer's solution (Fig. S4). Under current conditions, $SR1^+$ cells typically showed no responses to subthreshold stimuli but full-blown responses to suprathreshold stimuli (c.f. 20 vs. 30 psi). Although this prevented us to obtain full range dose–response relationship, suprathreshold stimuli elicited robust responses in $SR1^+$ Hana3A cells. These data strongly support that SR1 is sufficient to cause mechanosensitivity in its heterologous host cells.

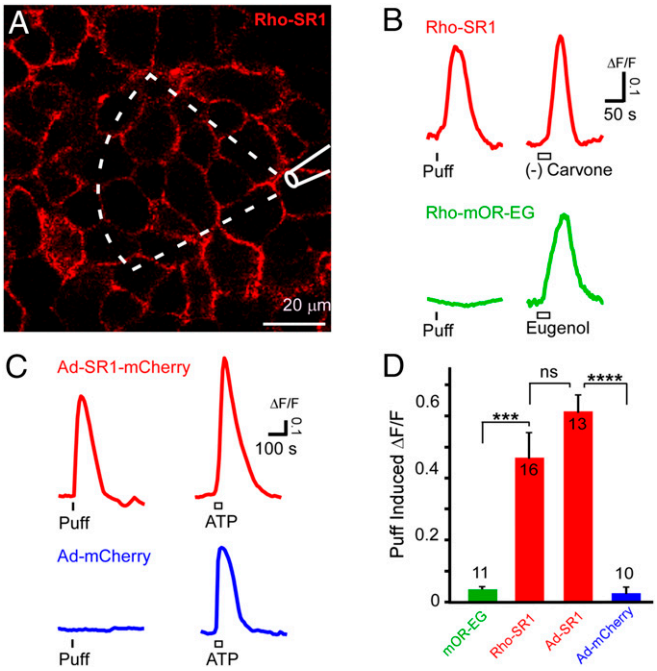

Fig. 5. Heterologous expression of SR1 is sufficient to cause mechanosensitivity in Hana3A cells. (*A*) Hana3A cells were transfected by the Rho-SR1 vector and immunostained by a Rho antibody in nonpermeable, live cells. The dashed sector indicates the area that is effectively stimulated by a puff from the pipette. Only cells within this sector are included for analysis. (*B*) Hana3A cells transfected by the Rho-SR1 vector showed elevated Ca^{2+} signals (measured as $\Delta F/F$) in response to puffs of Ringer's solution or bath perfusion of (–) carvone. Hana3A cells transfected by the Rho-mOR-EG vector did not respond to puffs of Ringer's solution but showed elevated Ca^{2+} signals to eugenol. (*C*) Hana3A infected by adenovirus (Ad) carrying SR1-IRES-mCherry (but not mCherry alone) responded to puffs of Ringer's solution. ATP was used as a positive control. (*D*) Summary of puff-induced responses from all four groups of Hana3A cells containing: mOR-EG, Rho-SR1, Ad-SR1, or Ad-mCherry only (***$P < 0.001$, ****$P < 0.0001$, ns = not significant in one-way ANOVA post hoc pairwise tests). All puffs of Ringer's solution were 1 s long at 30 psi, marked by vertical bars. Odorants and ATP (all at 100 μM) were applied through bath perfusion, marked by hollow rectangles.

Discussion

Collectively, our experiments strongly support that G protein-coupled ORs underlie mechanosensitivity of OSNs, revealing a surprising possibility that these receptors may be polymodal as both chemical and mechanical sensors. Five pieces of evidence substantiate this conclusion. First, blocking the odor transduction pathway by knocking out key signaling proteins (CNG channel or ACIII) or disrupting OR–G protein coupling completely eliminates both odor and mechanical responses (Figs. 1 and 2). Second, OSNs expressing different ORs display significantly different sensitivity to mechanical stimuli. For instance, SR1, M71 and I7 neurons show stronger mechanical responses than MOR23 and mOR-EG neurons (Fig. 2). Third, loss-of-function mutation of I7, genetic ablation of SR1, or genetic switch of M71 to β2AR completely abolishes or drastically reduces mechanical responses in the host OSNs (Figs. 2 and 4). Fourth, ectopic expression of the I7 receptor restores mechanosensitivity of loss-of-function I7-RDY cells (Fig. 4). Fifth, heterologous expression of SR1 confers mechanosensitivity to its host Hana3A cells (Fig. 5 and Fig. S4). Altogether, these data support the intriguing possibility that ORs serve as the mechanical sensors.

We suspect that without stimulation, ORs can spontaneously switch from inactive states to active states albeit at a low probability, which may determine the sensitivity of the receptors to mechanical stimuli. This notion is supported by two pieces of evidence. First, OSNs expressing different ORs have significantly different spontaneous firing rates (16, 32). OSNs expressing the inactive I7-RDY receptor completely lack spontaneous activity (Fig. 4; see also ref. 16), strongly suggesting that the spontaneous firing of an OSN originates from the spontaneous activation of its OR. Second, OSNs expressing the mechanosensory receptors (I7, M71, or SR1) have higher spontaneous firing rates than those expressing the nonmechanosensory receptors (MOR23 or mOR-EG) (16), indicating a higher predisposition of I7, M71 and SR1 for activating G protein. When mechanical stimulation deforms the cell membrane, it may cause enough conformational change in some ORs to stabilize the active state and trigger the transduction cascade. Further studies would be required to determine whether these mechanosensitive ORs have multiple active states, which might result from stimulation by different ligands or mechanical force. Another GPCR (angiotensin-II type-1) has been implicated as a stretch mechanosensor in vasoconstriction (26, 27) and more examples are emerging (3). Therefore, many GPCRs may be polymodal sensors that serve multiple functions in various cell types.

Puff-induced Ca^{2+} signals in Hana3A cells tend to show a full-blown response to any suprathreshold stimulation under the current experimental conditions. The inability of obtaining more detailed intensity-response relationship is presumably due to multistep amplifications, relatively coarse control of the stimulation, and slow kinetics of Ca^{2+} signals. Future experiments with enhanced sensitivity of Hana3A cells (e.g., via expression of a more permissive G protein), finer control of the stimulation, and

patch clamp recordings may allow comprehensive analysis of dose–response relationship.

In the main olfactory epithelium of wild-type animals, nearly 50% (18 of 37) of OSNs showed mechanical responses (4). This percentage should be considered as an upper limit because most of these cells were tested with pressures up to 50 psi. When tested by a lower pressure (20 psi), only 17% of the ΔSR1-RFP cells displayed mechanical responses (Fig. 4). Consistent with our findings, recordings from OSN axon terminals in awake, head-fixed rats revealed that 50% of all glomeruli showed inhalation-driven activities, but only 10% of them had strong responses (33). It is possible that ORs and their host OSNs form a continuous spectrum in terms of their mechanosensitivity and only a small fraction responds to mechanical stimuli carried by breathing or sniffing.

It is plausible that mechanosensitive cells may provide airflow information to the brain, which could be used to decode odor information (34–37). Indeed, a recent study using optogenetics demonstrates that mice are capable of detecting differences in light activation of OSNs when it is presented at specific phases of the respiratory cycle (38). The olfactory system may therefore use a population coding strategy that deciphers both odor and airflow information, based on the activities of OSNs that express different receptors of differing sensitivity to odorant and mechanical stimuli. Consistent with this notion, a subset of glomeruli and mitral/tufted cells (the projection neurons in the olfactory bulb) exhibits spontaneous activities coupled to respiration in the absence of odors (33, 39, 40). Because mitral/tufted cells project diffusely to cortical regions, OSNs may indirectly provide a driving force to synchronize the activity of these cortical regions with respiration and serve as a common clock that binds orofacial sensation (5, 41). We also speculate that respiration-related rhythmic activity may play a role in higher brain functions beyond sensory perception. The benefit of breathing through the nose instead of the mouth (such as during yoga or meditation practice) on the mind and body has been recognized for thousands of years. Our findings establish a molecular mechanism through which OSNs can send a peripheral afferent signal of breathing/sniffing to the brain.

Materials and Methods

Animals. Several genetically modified mouse lines were used in this study including transgenic I7-RDY-IRES-YFP (YFP, yellow fluorescent protein) line (Riken Bioresource Center RBRC02933) (15), transgenic mOR-EG-IRES-gapEGFP (18), gene-targeted MOR23-IRES-tauGFP, M71-IRES-tauGFP, mI7→M71-IRES-tauGFP, SR1-IRES-tauGFP, ΔSR1-RFP, and OMP-GFP (the coding region of olfactory marker protein is replaced by that of GFP) mice (19–21, 28). ACIII knockout mice ($ACIII^{-/-}$) and their littermate controls ($ACIII^{+/-}$ and $ACIII^{+/+}$) were as reported (10), and their genotypes were revealed only after the electrophysiological experiments. In gene-targeted OMP-IRES-I7 (ubiquitous I7) mice, all mature OSNs express the I7 receptor in addition to the endogenous ORs. Although the mouse lines were generated using embryos from mixed C57BL/6 × 129 or C57BL/6 × DBA2J background, they were all crossed to C57BL/6 mice for breeding. All experiments were performed on mice between 3 and 8 wk postnatal. All animal-handling procedures followed NIH guidelines and had been approved by the Institutional Animal Care and Use Committee.

Intact Olfactory Epithelial Preparation. The intact olfactory epithelia were prepared following published procedures (42, 43). Mice were deeply anesthetized by i.p. injection of a mixture of ketamine HCl and xylazine (200 and 20 mg/kg body weight, respectively) and decapitated. The head of each mouse was immediately put into ice-cold Ringer's solution, which contained 124 mM NaCl, 3 mM KCl, 1.3 mM $MgSO_4$, 2 mM $CaCl_2$, 26 mM $NaHCO_3$, 1.25 mM NaH_2PO_4, 15 mM glucose, pH 7.6, and 305 mOsm. The pH was kept at 7.4 after bubbling with 95%O_2/5%CO_2. The nose was dissected out en bloc and kept in oxygenated Ringer's solution. Before use, the entire mucosa attached to the nasal septum was peeled away from the underlying bone and transferred to a recording chamber. The preparation was continuously perfused with oxygenated Ringer's at room temperature (25 ± 2 °C).

Dissociation of OSNs. The olfactory mucosa from heterozygous OMP-GFP mice were dissected out in oxygenated divalent-free Ringer's solution and cut into small (1 mm × 1 mm) pieces. The tissue was then put in a 15 mL tube containing 2.5 mL of divalent-free Ringer's solution containing 20 mg/mL BSA (Sigma), 2 mg/mL collagenase, 80 mg of dispase (Gibco), and 25 μg/mL DNase II (Sigma) and incubated at 37 °C for 30 min. The divalent-free solution was replaced by normal Ringer's solution and the cells were triturated using a fire-polished pipette. Cells (400 μL) were plated onto Con A (10 mg/mL)-coated glass coverslips placed in 35-mm Petri dishes and allowed to settle. After 20 min, 1 mL of culture medium was added to each dish, and the dishes were placed at 37 °C in a CO_2 incubator for 1–24 h before use. The culture medium consisted of DMEM/F12 (Gibco) supplemented with 10% (vol/vol) fetal bovine serum (FBS), 100 μM ascorbic acid, 1× insulin–transferrin–selenium-X (Gibco), 2 mM glutamine, 100 U/mL penicillin, and 100 μg/mL streptomycin (Gibco).

Patch Clamp. In the intact olfactory epithelium, the dendritic knobs of the OSNs were visualized through an upright differential interference contrast microscope (Olympus BX51WI) equipped with a CCD camera (Dage-MTI) and a 40× water-immersion objective. An extra 4× magnification was achieved using an accessory lens in the light path. Fluorescence excitation was achieved by EXFO X-CITE 120 (Lumen Dynamics) and live images were captured by a cooled CCD camera (Sensicam QE, Cooke) combined with Metamorph software (Universal Imaging LLC). Superimposition of the images under bright field and fluorescent illumination permitted unambiguous identification of genetically labeled OSNs with GFP, YFP or RFP. Electrophysiological recordings were controlled by an EPC-10 amplifier combined with Pulse software (HEKA Electronic). Perforated patch-clamp was performed on the dendritic knobs by including 260 μM nystatin in the borosilicate glass pipette (resistance 15~20 MΩ), which was filled with the following solution: 70 mM KCl, 53 mM KOH, 30 mM methanesulfonic acid, 5.0 mM EGTA, 10 mM Hepes, 70 mM sucrose; pH 7.2 (KOH) and 310 mOsm. Under voltage-clamp mode, the signals were initially filtered at 10 kHz and then at 2.9 kHz. For voltage-gated ionic currents, the signals were sampled at 50 kHz. For odorant or pressure induced transduction currents (which are slow and long lasting), the signals were sampled at 4 kHz. Further filtering offline at 60 Hz did not change the response kinetics or amplitudes, indicating that the sampling rate was sufficient and signal aliasing was not a concern. Similarly, under current-clamp mode, the signals were filtered at 2.9 kHz and sampled at 5 kHz. Further filtering offline at 1.5 kHz did not change the response kinetics or amplitudes. Cell-attached patch was performed similarly but without including nystatin in the recording pipette. Recordings were started after the pipette formed a Giga-seal with the cell membrane, and the signals were filtered at 5 kHz and sampled at 10 kHz. The junction potential was ~10 mV and corrected in all experiments offline. For dissociated OSNs, the recording was performed on the cell body instead of the dendritic knob. Under voltage clamp mode, a positive response was defined as a peak current greater than 5 pA. Under cell-attached configuration, a positive response was identified for a particular trial if the instantaneous firing frequency of three or more continuous spikes exceeded the threshold (median instantaneous frequency + 5 spikes/s determined from the preceding 20 s epoch) within 2 s after onset of the stimulation. Instantaneous firing frequency was calculated as the inverse of the interspike interval (ISI) between consecutive action potentials (second to first, third to second, and so forth). For wild-type I7 neurons, puff-induced responses were calculated as the average instantaneous firing frequency from the initial burst ("*b*" in Fig. 2*B*), while the basal activity was from the preceding 20 s epoch. For I7-RDY neurons, due to the lack of stimulation elicited responses, the average instantaneous firing frequency from the first five spikes (the average number of spikes during a puff-induced burst) after onset of the puff was compared with that in the preceding 20 s epoch (Fig. 2*H*).

Odorants and isoproterenol were prepared as 0.5 M stock solutions in dimethyl sulfoxide (DMSO) and kept at −20 °C. IBMX was prepared as a 20 mM stock solution containing 20% (vol/vol) DMSO in water. The odor mixture (Mix 1) contained 19 compounds at equal molar concentration: heptanol, octanol, hexanal, heptanal, octanal, heptanoic acid, octanoic acid, cineole, amyl acetate, (+) limonene, (–) limonene, (+) carvone, (–) carvone, 2-heptanone, anisaldehyde, benzaldehyde, acetophenone, 3-heptanone, and ethyl vanillin. Final solutions were made before each experiment by adding Ringer's solution. All chemicals and odorants were purchased from Sigma-Aldrich except lyral, a generous gift from International Flavors and Fragrances.

Heterologous Expression. Hana3A cells, a modified HEK293 cell line, stably express RTP1L (receptor-transporting protein 1L), RTP2, REEP1 (receptor expression-enhancing protein 1), and $G_{\alpha olf}$ to facilitate OR surface expression (44). Hana3A cells were grown in MEM (Cellgro), supplemented with 10% (vol/vol) FBS (Cellgro), 100 μg/mL penicillin-steptomycin (Invitrogen), 1.25 g/mL amphotericin (Sigma), and 1 μg/mL puromycin (Sigma). The cells were cultured at 37 °C under a humidified atmosphere containing 5%

(vol/vol) CO_2. Confluent cells were transfected with pCI-Rho-SR1 or pCI-Rho-mOR-EG and RTP1S by Lipofectamine 2000 (Invitrogen). The Rho-tag (the sequence encoding the first 20 amino acids of rhodopsin) was added before the N terminus of the receptor gene to facilitate OR surface expression, which can be confirmed by live-cell immunocytochemistry. Briefly, the transfected cells were incubated with the primary antibody (mouse monoclonal anti-Rhodopsin 4D2, Abcam; 1:100) on ice for 1 h. After rinsing for three times, the secondary antibody (Cy3-conjucated anti-mouse IgG; 1:200) was added and the cells were incubated for 45 min on ice. The cells were then fixed with 2% (wt/vol) paraformaldehyde in PBS and mounted with Vectashield mounting medium (Vector Laboratories).

The adenovirus (E1/E3-deleted, type 5) carrying SR1-IRES-mCherry or mCherry alone was constructed under the cytomegalovirus promoter. Virus was amplified in HEK293 cells and purified by cesium chloride step-gradient ultracentrifugation (Vector Biolabs). For viral infection, hana3A cells seeded on 24-well plates were infected with 2×10^6 pfu adenovirus.

Calcium Imaging. Twenty-four hours after DNA transfection or viral infection, cells were loaded with 5 μM fluo-4/AM (Invitrogen) for 40 min at 37 °C. Cultured cells on coverslips were rinsed with Hepes buffered Ringer's solution (5 mM KCl, 145 mM NaCl, 2 mM CaCl2, 5 mM glucose, 1 mM $MgCl_2$, 1 mM sodium pyruvate and 20 mM Hepes, adjusted to pH 7.4) for 15 min before the recording. Odorant or ATP was bath perfused for ~30 s and mechanical stimulation was described below. There were at least three minutes between any two stimuli. Lambda DG-4 (Sutter Instrument Company) combined with a GFP filter cube mounted on a BX61WI microscope was used to provide excitation (around 488 nm) and collect emitted light (around 515 nm). The fluorescent signals were acquired by a cooled CCD camera (SensiCam QE; Cooke), controlled by the MetaFluor software. Images were collected every 4 s and $\Delta F/F$ was calculated as $(Fr - F)/F$, where Fr was the response to a stimulus at any time point and F was baseline activity, obtained by averaging 10 frames before stimulation.

Mechanical Stimulation. A puffing pipette (single- or multibarrel) was placed ~25 μm downstream from the recording site, to deliver stimuli by pressure ejection through a picospritzer (Pressure System IIe). Odorant or mechanical stimuli were delivered at different pressure levels (0–60 psi) with a pulse length of 300 ms to 1 s. By including food dye in the puffing pipette, we analyzed the liquid flow rates caused by puffs at different pressures via video recording and found a roughly linear relationship between the flow rate (fl) and pressure (p): $fl = 13p + 272$ ($P < 0.01$ in regression analysis). At the recording site, with increasing pressure from 5, 20, to 60 psi, the puffs generated increasing flow rates from 300, 600, to 1080 μm/s, respectively. The shear stress delivered by a puff can be estimated according to *shear stress* = (dV/dy)·μ, in which dV is the fluid velocity change along the preparation, dy is the height of the puffing pipette above the preparation (~3 μm), and μ is viscosity (8.90×10^{-4} Pascal·s for water). Therefore, a 5-, 20-, or 60-psi puff is equivalent to a shear stress of 0.089, 0.178, or 0.320 Pa. These numbers are within the physiological range of shear stress in rodent nose (up to 1 Pa in the septal organ which has the fastest airflow rate among the olfactory regions) based on a computational fluid dynamics model (45).

ACKNOWLEDGMENTS. We thank Drs. Haiqing Zhao and Randall Reed for providing ubiquitous I7 mice, Drs. Joel Mainland and Hiroaki Matsunami for Hana3A cells, and Dr. Kazushige Touhara for the mOR-EG plasmid. This work was supported by grants from the National Institute on Deafness and Other Communication Disorders, NIH (R01DC006213 and R01DC011554).

1. Delmas P, Coste B (2013) Mechano-gated ion channels in sensory systems. *Cell* 155(2): 278–284.
2. Eijkelkamp N, Quick K, Wood JN (2013) Transient receptor potential channels and mechanosensation. *Annu Rev Neurosci* 36:519–546.
3. Storch U, Mederos y Schnitzler M, Gudermann T (2012) G protein-mediated stretch reception. *Am J Physiol Heart Circ Physiol* 302(6):H1241–H1249.
4. Grosmaitre X, Santarelli LC, Tan J, Luo M, Ma M (2007) Dual functions of mammalian olfactory sensory neurons as odor detectors and mechanical sensors. *Nat Neurosci* 10(3):348–354.
5. Kleinfeld D, Deschênes M, Wang F, Moore JD (2014) More than a rhythm of life: breathing as a binder of orofacial sensation. *Nat Neurosci* 17(5):647–651.
6. Buck L, Axel R (1991) A novel multigene family may encode odorant receptors: a molecular basis for odor recognition. *Cell* 65(1):175–187.
7. Zhang X, Zhang X, Firestein S (2007) Comparative genomics of odorant and pheromone receptor genes in rodents. *Genomics* 89(4):441–450.
8. Su CY, Menuz K, Carlson JR (2009) Olfactory perception: receptors, cells, and circuits. *Cell* 139(1):45–59.
9. Mori K, Sakano H (2011) How is the olfactory map formed and interpreted in the mammalian brain? *Annu Rev Neurosci* 34:467–499.
10. Wong ST, et al. (2000) Disruption of the type III adenylyl cyclase gene leads to peripheral and behavioral anosmia in transgenic mice. *Neuron* 27(3):487–497.
11. Chen X, Xia Z, Storm DR (2012) Stimulation of electro-olfactogram responses in the main olfactory epithelia by airflow depends on the type 3 adenylyl cyclase. *J Neurosci* 32(45):15769–15778.
12. Scheer A, Fanelli F, Costa T, De Benedetti PG, Cotecchia S (1996) Constitutively active mutants of the alpha 1B-adrenergic receptor: role of highly conserved polar amino acids in receptor activation. *EMBO J* 15(14):3566–3578.
13. Kobilka BK, Deupi X (2007) Conformational complexity of G-protein-coupled receptors. *Trends Pharmacol Sci* 28(8):397–406.
14. Sakmar TP, Franke RR, Khorana HG (1989) Glutamic acid-113 serves as the retinylidene Schiff base counterion in bovine rhodopsin. *Proc Natl Acad Sci USA* 86(21):8309–8313.
15. Imai T, Suzuki M, Sakano H (2006) Odorant receptor-derived cAMP signals direct axonal targeting. *Science* 314(5799):657–661.
16. Connelly T, Savigner A, Ma M (2013) Spontaneous and sensory-evoked activity in mouse olfactory sensory neurons with defined odorant receptors. *J Neurophysiol* 110(1):55–62.
17. Savigner A, et al. (2009) Modulation of spontaneous and odorant-evoked activity of rat olfactory sensory neurons by two anorectic peptides, insulin and leptin. *J Neurophysiol* 101(6):2898–2906.
18. Oka Y, et al. (2006) Odorant receptor map in the mouse olfactory bulb: in vivo sensitivity and specificity of receptor-defined glomeruli. *Neuron* 52(5):857–869.
19. Vassalli A, Rothman A, Feinstein P, Zapotocky M, Mombaerts P (2002) Minigenes impart odorant receptor-specific axon guidance in the olfactory bulb. *Neuron* 35(4):681–696.
20. Grosmaitre X, et al. (2009) SR1, a mouse odorant receptor with an unusually broad response profile. *J Neurosci* 29(46):14545–14552.
21. Bozza T, Feinstein P, Zheng C, Mombaerts P (2002) Odorant receptor expression defines functional units in the mouse olfactory system. *J Neurosci* 22(8):3033–3043.
22. Tian H, Ma M (2004) Molecular organization of the olfactory septal organ. *J Neurosci* 24(38):8383–8390.
23. Fuss SH, Zhu Y, Mombaerts P (2013) Odorant receptor gene choice and axonal wiring in mice with deletion mutations in the odorant receptor gene SR1. *Mol Cell Neurosci* 56:212–224.
24. Feinstein P, Bozza T, Rodriguez I, Vassalli A, Mombaerts P (2004) Axon guidance of mouse olfactory sensory neurons by odorant receptors and the beta2 adrenergic receptor. *Cell* 117(6):833–846.
25. Omura M, Grosmaitre X, Ma M, Mombaerts P (2014) The β2-adrenergic receptor as a surrogate odorant receptor in mouse olfactory sensory neurons. *Mol Cell Neurosci* 58:1–10.
26. Mederos y Schnitzler M, et al. (2008) Gq-coupled receptors as mechanosensors mediating myogenic vasoconstriction. *EMBO J* 27(23):3092–3103.
27. Zou Y, et al. (2004) Mechanical stress activates angiotensin II type 1 receptor without the involvement of angiotensin II. *Nat Cell Biol* 6(6):499–506.
28. Potter SM, et al. (2001) Structure and emergence of specific olfactory glomeruli in the mouse. *J Neurosci* 21(24):9713–9723.
29. Saito H, Chi Q, Zhuang H, Matsunami H, Mainland JD (2009) Odor coding by a Mammalian receptor repertoire. *Sci Signal* 2(60):ra9.
30. Saito H, Kubota M, Roberts RW, Chi Q, Matsunami H (2004) RTP family members induce functional expression of mammalian odorant receptors. *Cell* 119(5):679–691.
31. Zhuang H, Matsunami H (2007) Synergism of accessory factors in functional expression of mammalian odorant receptors. *J Biol Chem* 282(20):15284–15293.
32. Reisert J (2010) Origin of basal activity in mammalian olfactory receptor neurons. *J Gen Physiol* 136(5):529–540.
33. Carey RM, Verhagen JV, Wesson DW, Pírez N, Wachowiak M (2009) Temporal structure of receptor neuron input to the olfactory bulb imaged in behaving rats. *J Neurophysiol* 101(2):1073–1088.
34. Buonviso N, Amat C, Litaudon P (2006) Respiratory modulation of olfactory neurons in the rodent brain. *Chem Senses* 31(2):145–154.
35. Schaefer AT, Margrie TW (2007) Spatiotemporal representations in the olfactory system. *Trends Neurosci* 30(3):92–100.
36. Wachowiak M (2011) All in a sniff: olfaction as a model for active sensing. *Neuron* 71(6):962–973.
37. Uchida N, Kepecs A, Mainen ZF (2006) Seeing at a glance, smelling in a whiff: rapid forms of perceptual decision making. *Nat Rev Neurosci* 7(6):485–491.
38. Smear M, Shusterman R, O'Connor R, Bozza T, Rinberg D (2011) Perception of sniff phase in mouse olfaction. *Nature* 479(7373):397–400.
39. Onoda N, Mori K (1980) Depth distribution of temporal firing patterns in olfactory bulb related to air-intake cycles. *J Neurophysiol* 44(1):29–39.
40. Phillips ME, Sachdev RN, Willhite DC, Shepherd GM (2012) Respiration drives network activity and modulates synaptic and circuit processing of lateral inhibition in the olfactory bulb. *J Neurosci* 32(1):85–98.
41. Ito J, et al. (2014) Whisker barrel cortex delta oscillations and gamma power in the awake mouse are linked to respiration. *Nat Commun* 5:3572.
42. Ma M, Chen WR, Shepherd GM (1999) Electrophysiological characterization of rat and mouse olfactory receptor neurons from an intact epithelial preparation. *J Neurosci Methods* 92(1-2):31–40.
43. Grosmaitre X, Vassalli A, Mombaerts P, Shepherd GM, Ma M (2006) Odorant responses of olfactory sensory neurons expressing the odorant receptor MOR23: A patch clamp analysis in gene-targeted mice. *Proc Natl Acad Sci USA* 103(6):1970–1975.
44. Zhuang H, Matsunami H (2008) Evaluating cell-surface expression and measuring activation of mammalian odorant receptors in heterologous cells. *Nat Protoc* 3(9):1402–1413.
45. Jiang J, Zhao K (2008) Quantifying mechanical stimuli in rat and human nose models during breathing. *Chem Senses* 33:S106.